nature electronics

ARTICLES

https://doi.org/10.1038/s41928-019-0257-7

Wireless body sensor networks based on metamaterial textiles

Xi Tian[1,6], Pui Mun Lee[1,6], Yu Jun Tan[2,3], Tina L. Y. Wu[4], Haicheng Yao[2], Mengying Zhang[1], Zhipeng Li[1], Kian Ann Ng[5], Benjamin C. K. Tee[2,3,5] and John S. Ho[1,3,5*]

Wireless networks of sensors, displays and smart devices that can be placed on a person's body could have applications in health monitoring, medical interventions and human–machine interfaces. Such wireless body networks are, however, typically energy-inefficient and vulnerable to eavesdropping because they rely on radio-wave communications. Here, we report energy-efficient and secure wireless body sensor networks that are interconnected through radio surface plasmons propagating on metamaterial textiles. The approach uses clothing made from conductive fabrics that can support surface-plasmon-like modes at radio communication frequencies. Our body sensor networks enhance transmission efficiencies by three orders of magnitude compared to conventional radiative networks without the metamaterial textile, and confine wireless communication to within 10 cm of the body. We also show that the approach can offer wireless power transfer that is robust to motion and textile-based wireless touch sensing.

Over the past decade, sensors, displays and smart devices have been developed that can be seamlessly integrated onto the human body[1–8]. Connecting these devices into a functional and practical network is, however, challenging[9,10]. For example, direct wiring between sensor nodes is widely used in clinical and research settings, but such an approach is not well suited to continuous use because it disrupts physical activity. Furthermore, recent advances in wearable electronics have shown that sensors and conductive wires can be integrated into clothing[11,12] or onto skin[13], but interconnecting them with other electronic devices for power supply and data collection remains difficult.

To create an unconstrained network of discrete devices, wireless interconnection approaches are required. However, wireless technologies and protocols for body networks[14,15] rely on the transmission of radio-waves into the surrounding space, and are therefore energy-consuming and vulnerable to interception by others. These limitations impose hardware and software requirements that limit the size, lifetime and function of body-based sensors. For example, low-power circuits and energy storage may be needed to address the power consumption issues, while security protocols and cryptography may be required to ensure privacy[16].

In contrast to radio-waves, electromagnetic waves at optical frequencies can be confined on metallic surfaces in localized excitations called surface plasmons[17]. Because these modes can propagate conformably along the surface, and interact strongly with nearby objects through an evanescent field, they are widely used as interconnection elements in integrated photonic devices[18]. Although surface plasmons do not exist in natural materials at radio-frequencies, metamaterial approaches have shown that these electromagnetic modes can be engineered by designing structured conductive surfaces such as textured metal sheets[19], wire arrays[20] and flexible printed circuit boards[21].

In this Article, we show that clothing structured with conductive textiles—termed metamaterial textiles—can support surface-plasmon-like modes at communication frequencies and thus provide a platform for the propagation of radio-waves around the body (Fig. 1a). With this approach, we develop energy-efficient and secure wireless body sensor networks interconnected by radio surface plasmons propagating on metamaterial textiles. Unlike conventional electronic textiles, our metamaterial textiles (Fig. 1b) can achieve interconnection of devices by contactless proximity to the body without requiring them to be 'plugged in'. In particular, when standard wireless devices are placed near metamaterial textiles, their interconnection can be achieved through the propagation of wireless signals as surface waves instead of wireless signals radiating into the surrounding space (Fig. 1c). The physical localization of wireless signals onto the body (Fig. 1d) can enable personal sensor networks that are highly efficient, immune to interference, and inherently secure.

Our metamaterial textiles can support the propagation of wireless signals around the body and are also robust to daily wear, having no active electronic components. We show that the transmission efficiency of wireless networks interconnected through such metamaterial textiles can be enhanced by over three orders of magnitude (>30 dB) compared to conventional radiative networks without the metamaterial textile, and that wireless communication can be localized within 10 cm of the body. We also demonstrate that our metamaterial textiles can be used to power sensors wirelessly and for touch sensing via wireless signals.

Metamaterial textile design

We first examine the conditions required for a metamaterial to support radio-frequency waves while bound to the surface of the body. We consider a model of the interface between air and the body consisting of a half-space that is free-space in the upper region ($z > 0$) and filled with biological material with a relative dielectric permittivity ε_{body} in the lower region ($z < 0$). Taking x to be the direction of propagation, a thin planar metamaterial placed on the interface

[1]Department of Electrical and Computer Engineering, National University of Singapore, Singapore, Singapore. [2]Department of Materials Science and Engineering, National University of Singapore, Singapore, Singapore. [3]Institute for Health Innovation and Technology, National University of Singapore, Singapore, Singapore. [4]Department of Systems Design Engineering, University of Waterloo, Waterloo, Ontario, Canada. [5]The N.1 Institute for Health, National University of Singapore, Singapore, Singapore. [6]These authors contributed equally: Xi Tian, Pui Mun Lee. *e-mail: johnho@nus.edu.sg

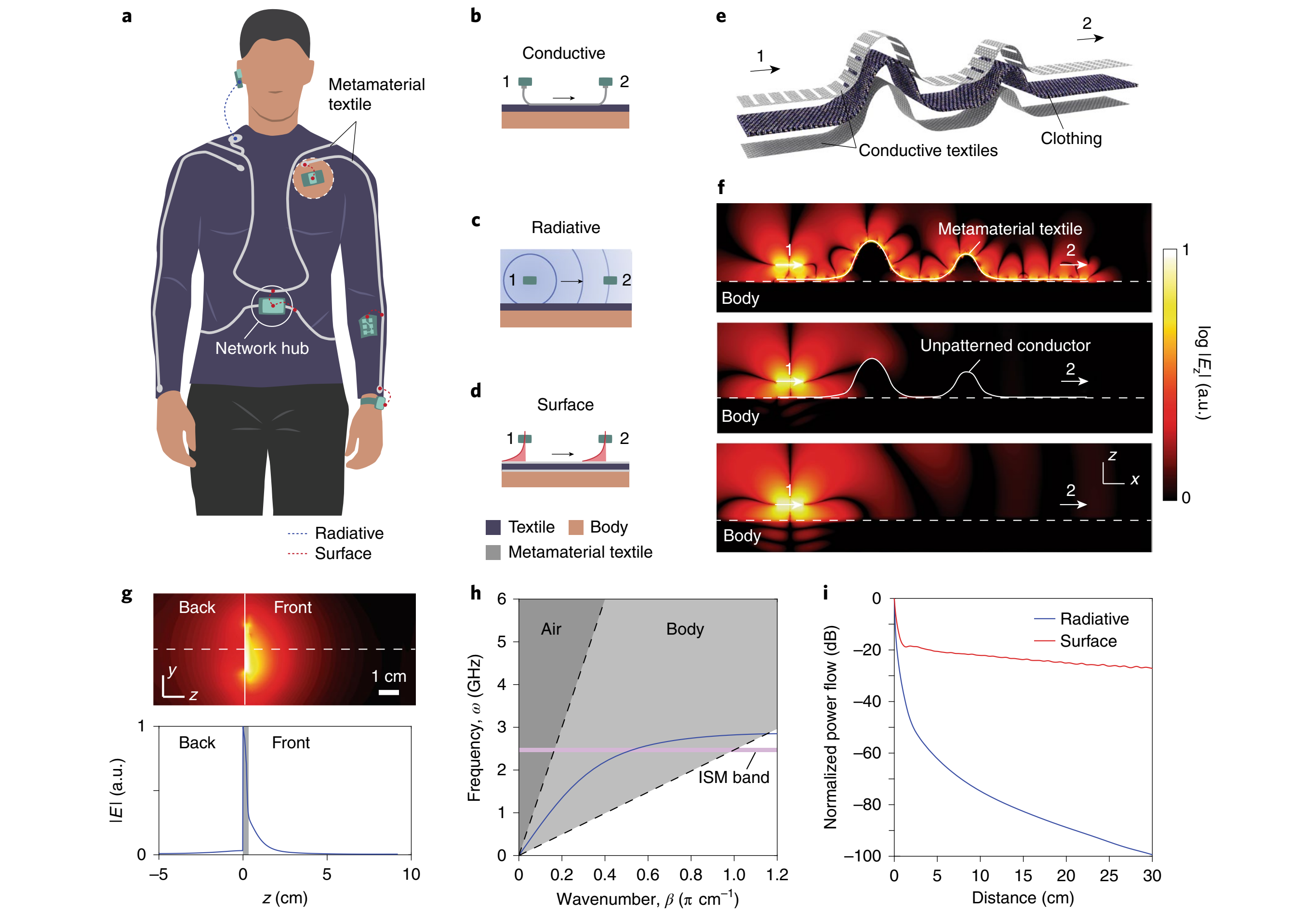

Fig. 1 | Wireless body sensor networks with metamaterial textiles. a, Illustration of a sensor network interconnected by radio surface plasmons on clothing. **b**–**d**, Comparison with conductive and radiative interconnections. Conductive interconnects (**b**) require devices to be physically connected (grey line), while radiative interconnection (**c**) is wireless but transmits inefficiently and insecurely into the surrounding space (blue lines). In contrast, interconnection with surface waves (**d**) is contactless but requires proximity to the body (red lines). **e**, Structure of the metamaterial textile. **f**, Electric field distribution $|E_z|$ emitted by a dipole above a metamaterial textile (top), unpatterned conductive textile (centre) and non-conductive textile (bottom). The textile is placed on an air–body half-space with $\varepsilon_{\text{body}} = 40$. **g**, Top, normalized field distribution on the y–z plane; bottom, field profile along the dashed line in the field distribution. **h**, Dispersion curve of the metamaterial structure. The dark shaded area shows the radiation cone in air, the light shaded area shows the radiation cone in the body, and the shaded purple area shows the 2.4–2.5 GHz ISM band. **i**, Comparison of the normalized power flow (peak value of the Poynting vector) with distance from the transmitter near the textile (confined, surface) and in free-space (radiative).

$z = 0$ supports a mode whose electric field in the upper ($\mathbf{E}_1$) and lower ($\mathbf{E}_2$) region is given by

$$\mathbf{E}_n(\mathbf{r}, t) = E_0 \begin{pmatrix} i\alpha_n/\beta \\ 0 \\ 1 \end{pmatrix} e^{i\beta x - \alpha_n |z| - i\omega t} \tag{1}$$

where E_0 is the field amplitude, ω the frequency, β the wavenumber and α_n the decay parameter in each region. The form of equation (1) is dictated by symmetry considerations, while the design of the metamaterial determines the relationships between the parameters β, ω and α_n. For a plasmonic metamaterial, β and ω are related by a surface plasmon dispersion relation, whose curve lies to the right of the light line $\beta = \omega/c$, where c is the speed of light, and approaches an asymptotic limit termed the surface plasma frequency (see Methods). The decay parameter for the free-space region is given by $\alpha_1 = \sqrt{\beta^2 - (\omega/c)^2}$, which, together with the dispersion relation, implies that the mode is bound to the upper surface because α_1 is purely real. The lower region, however, supports additional bulk radiative modes within the region $\beta < \omega\sqrt{\varepsilon_{\text{body}}}/c$ due to the presence of biological tissue. Remarkably, these modes encompass nearly all frequencies below the surface plasma frequency because of the very high dielectric permittivity of biological tissue at radiofrequencies. To allow bound surface modes to exist on the body, the metamaterial should therefore support a single-sided mode $\alpha_2 \to \infty$ to prevent coupling to these bulk radiative modes and leakage into the lower region.

In addition to supporting surface modes, the metamaterial must also be able to interact with nearby sensors and devices without physical contact. The interaction of the surface waves with a wireless device can be described by expanding the electric field into forward (+) and backward (−) propagating surface modes $\mathbf{E}(\mathbf{r},t) = (a_+\mathbf{e}_+(\mathbf{r}) + a_-\mathbf{e}_-(\mathbf{r}))e^{-i\omega t}$, where $a_\pm$ are the mode amplitudes and $\mathbf{e}_\pm(\mathbf{r}) = p(y)(i\alpha_n/\beta, 0, 1)e^{\pm i\beta x - \alpha_n|z|}$ are the mode field patterns with a normalized profile function $\frac{1}{2}\int |p(y)|^2\,\mathrm{d}y = \frac{\alpha_1\alpha_2}{\alpha_1+\alpha_2}$. When a radiofrequency source with current density $\mathbf{j}(\mathbf{r})$ is placed above the body, the modes are excited with amplitude[22]

$$a_{\pm} = -\frac{\beta}{2\omega\varepsilon_0}\int \mathbf{j}(\mathbf{r})\cdot\mathbf{e}_{\mp}(\mathbf{r})\mathrm{d}^3 r \quad (2)$$

Since $\mathbf{e}_{\pm}(\mathbf{r})$ extends evanescently in the z direction, contactless excitation is efficient within a distance comparable to the decay length α_1^{-1} above the surface. In contrast, conventional waveguides, such as coaxial cables and microstrip lines, lack such an evanescent field and typically cannot be efficiently excited by nearby sources without specialized connectors. The metamaterial can interact with a standard wireless device through the current density $\mathbf{j}(\mathbf{r})$ generated by its built-in antenna without any modification, although it should be noted that the excitation does not depend on conventional performance metrics such as directivity and gain. The orientation dependence of the interaction can be evaluated by approximating $\mathbf{j}(\mathbf{r})$ by its electric dipole moment $\mathbf{p}$ centred at $\mathbf{r}_0$. Equation (2) then reduces to $a_{\pm} = \frac{i\beta}{2\varepsilon_0}[\mathbf{p}\cdot\mathbf{e}_{\mp}(\mathbf{r}_0)]$, which shows that the dipole excites surface waves as long as it has a non-zero longitudinal (x) or vertical (z) component, because surface plasmon-like modes are transverse-magnetic.

Based on these physical considerations, the metamaterial must satisfy the following strict requirements to interconnect wireless networks with surface plasmon-like modes: (1) it must support a surface plasmon dispersion relation with cutoff frequency above the 2.4–2.5 GHz industrial, scientific and medical (ISM) band, (2) the field in the lower region must be screened such that $\alpha_2 \to \infty$ to minimize coupling with the body and (3) the wavenumber β of the surface modes must correspond to a decay length α_1^{-1} on the order of a few centimetres. These conditions are not met with existing metamaterials based on metal sheets or printed circuit boards. To develop a textile platform that meets these requirements, we designed a metamaterial using a numerical optimization procedure for the planar structure in Fig. 1e (see Methods and Supplementary Fig. 1). This metamaterial structure consists of a planar comb-shaped pattern on the top layer (previously used as a plasmonic metamaterial[21,23]), an intermediate fabric layer and a bottom layer comprising an unpatterned metallic conductor. The design procedure yields geometrical parameters such that the combined structure supports a surface plasmon dispersion that satisfies the requirements for wireless networking and has overall dimensions (2.5 cm width, 8 mm unit cell length) compatible with easy integration with most types of clothing by direct attachment of commercially available, low-cost conductive textiles.

Figure 1f shows wireless excitation of the surface modes on metamaterial textiles by a horizontal dipole transmitter placed 5 mm above the structure. The transmission efficiency to the receiver is more than three orders of magnitude higher than radiative transmission performed without the metamaterial textile. The unpatterned conductive textiles, in contrast, do not support surface modes and result in efficiencies comparable to radiative transmission. The fraction of energy transmitted into surface modes versus radiative modes is controlled by the distance of the dipole from the metamaterial textile, with preferential coupling to surface modes within 15 mm of the surface (Supplementary Fig. 2). Their propagation is also highly robust to folding and bending, and incurs minimal radiative losses and reflection with curvature (<5% for a U-turn with 1.25 mm radius-of-curvature; Supplementary Fig. 3). The surface plasmon-like nature of the modes is confirmed by the exponential field decay (Fig. 1g) and asymptotic dispersion curve (Fig. 1h), which fit the surface plasmon dispersion model (see Methods). Propagation losses are dictated by the textile conductivity and are estimated to be less than 0.2 dB cm^{-1} for moderate conductivities ($\sigma > 2\times10^5$ S m^{-1}) (Fig. 1i and Supplementary Fig. 4).

Metamaterial textiles provide a versatile platform for manipulating wave propagation around the body. Their geometrical parameters (Fig. 2a) can be tuned to achieve surface modes with wavenumbers β ranging from 0.35π to 0.65π rad cm^{-1} (Fig. 2b) and corresponding decay lengths α_1^{-1} ranging from 5 to 10 mm (Fig. 2c) at 2.4 GHz. Using a design with $\beta = 0.5\pi$ cm^{-1}, we demonstrate three basic building blocks for more complex wave circuits—a power divider, antenna and ring resonator—integrated into a network on a cotton–polyester shirt (Fig. 2d). The devices are fabricated by laser-cutting conductive textile (Cu/Ni polyester) and attaching the patterns with fabric adhesive. The power splitter evenly divides an input signal between the two output ports, enabling the distribution and combination of signals from multiple devices. Device functionality is validated by the close agreement between numerical simulations and near-field measurements (Fig. 2e) as well as port measurements on the body (Fig. 2h). The antenna launches an input signal confined on the textile surface as radiation into the surrounding space for short-range transmission, such as from the shoulder to an ear-worn device. Simulations and field mapping show excitation of a resonant antenna mode (Fig. 2f), and measurements from a receiver placed 10 cm above the antenna indicate radiation within the 2.4–2.5 GHz band (Fig. 2i). Finally, the ring resonator exhibits a series of resonances that can be used to filter signals, sense mechanical strain and enhance interactions with nearby objects. Simulations and field mapping reveal a whispering gallery mode of order $m = 7$ at 2.5 GHz (Fig. 2g), which corresponds to a sharp resonant dip in the transmission spectrum between probes placed at two diametrically opposite points (Fig. 2j). The resonant frequency measurably shifts as the textile is stretched (Supplementary Fig. 5), providing a potential mechanism for wirelessly sensing textile strain. Close agreement between measurements on and off the body demonstrate robustness to environmental effects (Supplementary Fig. 6). Circuits built from these basic devices may potentially perform sophisticated functions for applications in energy transfer, sensing and signal processing on a wearable platform[24,25].

Unlike conventional conductive textiles, signal propagation on metamaterial textiles is robust to discontinuities in the underlying conductive structure. Simulations show that the transmission efficiency across a 1 cm gap in the direction of propagation (x) is greater than −7 dB; the structures can also be discontinuous in the transverse (y) or vertical (z) directions with transmission efficiencies greater than −3 dB and −10 dB, respectively, for a 1 cm gap (Supplementary Fig. 7). Experimental measurements of wireless Bluetooth transmission along the metamaterial textile show a comparable transmission efficiency for a vertical gap as well as no detectable decrease in signal strength when the textile is cut at multiple locations (Supplementary Fig. 8). Such contactless transmission along the metamaterial textiles allows signals to efficiently couple between nearby structures and propagate from one article of clothing to another.

Energy-efficient communication

We next investigated the ability of the metamaterial textile to enhance the transmission of wireless signals between devices worn on the body. Figure 3a shows a network of two sensor nodes, consisting of commercial Bluetooth modules attached to the left shoulder and lower back, and a central hub (smartphone) worn on the abdomen. Full-wave simulations of the sensors transmitting in a computational body model show confinement of energy onto the textile surface and propagation around the curvature of the body (Fig. 3b). In contrast, radiative communication performed in the absence of the metamaterial textile results in about three orders of magnitude lower efficiency due to radiative losses and obstruction by the body. To evaluate the robustness of the enhancement, real-time monitoring of the signal strength was performed with healthy volunteers wearing two sensors and a smartphone during physiological activity (see Methods). Controls with the conventional radiative network were conducted by repeating the activity protocol without the metamaterial textile.

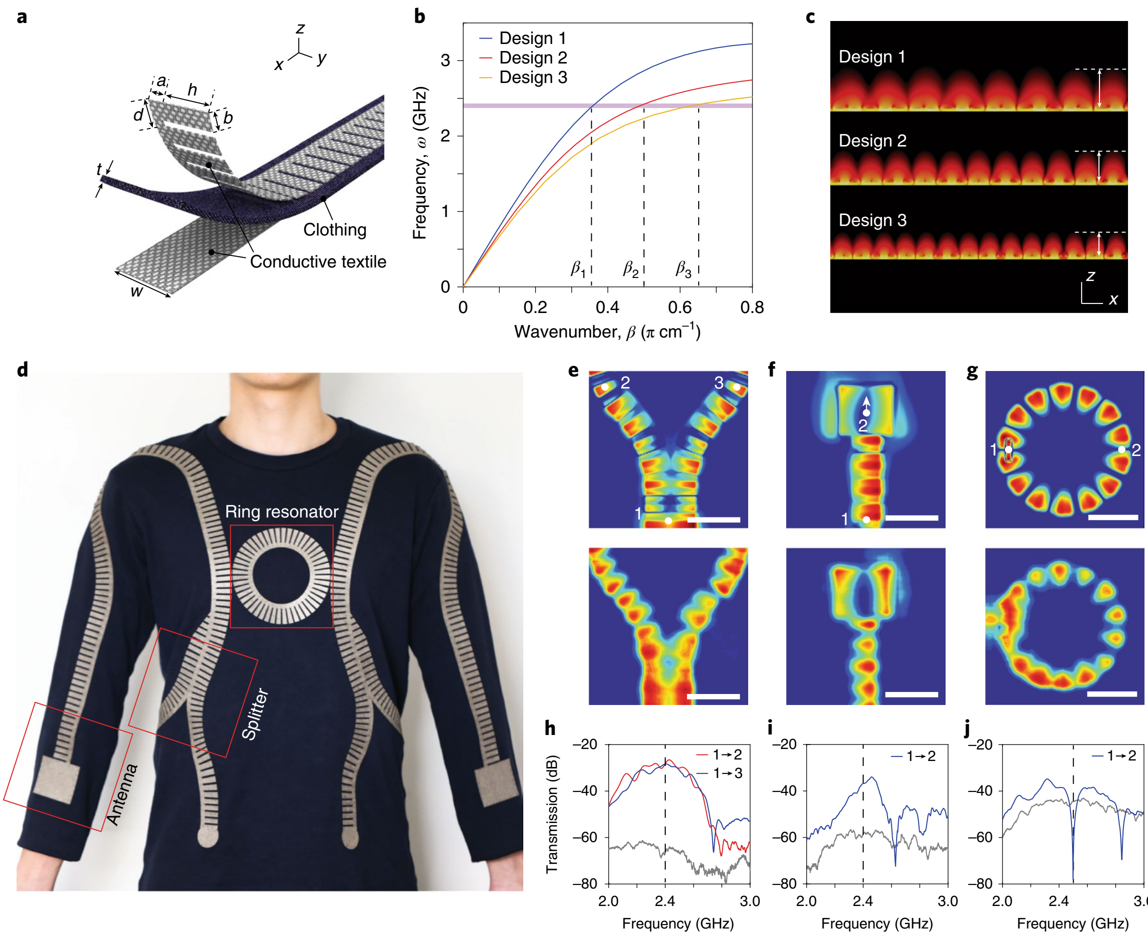

Fig. 2 | Design of metamaterial textiles and wave devices. a, Metamaterial textile structure and geometrical design parameters. **b**, Dispersion curves for three optimized designs with $h = 17$ mm, 21 mm and 23 mm, respectively. **c**, Electric field profile of the surface mode supported by designs with decay lengths $\alpha_1^{-1} = 10$, 7 and 5 mm, respectively (white dashed lines show $3\alpha_1^{-1}$). **d**, Metamaterial textile network integrating splitters, antennas and a ring-resonator based on design 2. **e**–**g**, Simulations (top) and near-field measurements (bottom) of the normal component of the electric field above the textile surface during continuous-wave excitation at position 1 with a dipole probe. Scale bars, 5 cm. **h**–**j**, Transmission spectra between antennas placed 5 mm above the positions labelled in **e**–**g** on the body. Grey lines show radiative transmission spectra measured without the metamaterial textiles. The white arrow in **f** indicates measurement of the radiative field with a probe placed 10 cm above the textile.

Figure 3c shows that the relative signal strength indicator (RSSI) from one subject during 5 min intervals of standing, walking and running was enhanced by ~31 dB for both devices. Across a group of subjects ($n = 3$), the enhancement in RSSI averaged over each activity was 32.1 dB for the shoulder device and 32.7 dB for the back device (Fig. 3d). This enhancement of the signal transmission efficiency by three orders of magnitude translates into lower power consumption and higher data throughput. In particular, the metamaterial textile enables operation of the sensor at the lowest available transmit power setting (−55 dBm) without significant increase in packet latency (Fig. 3e). In contrast, connection could not be established at power levels below −20 dBm in the absence of the textile. Cumulative measurements show a rate of 4.53 packets per second for the radiative network and 31.86 packets per second for the metamaterial textile network at the lowest power setting where connection could be established (Fig. 3f). Lowering the transmit power enables significantly prolonged sensor battery lifetimes as wireless communication is one of the most energy-demanding functions performed by the sensor[26,27]. Battery-powered sensor nodes operated reliably for ~40 h during continuous radiative Bluetooth transmission, whereas sensor nodes interconnected via metamaterial textiles could operate well beyond 70 h because of the reduced transmit power (Fig. 3g).

Secure wireless communication

Data security is essential for the transmission of health and other personal data within body networks. Conventional wireless systems, however, are vulnerable to eavesdropping because signal transmission from sensor nodes on the body to another relies on radiation into the surrounding space. Due to obstruction by the body, the range at which a radiative signal can be intercepted is generally much larger than the separation distance between the devices. As an illustrative example, we performed full-wave simulations of radiative propagation from a transmit node on the abdomen to a receiver node on the back (Supplementary Fig. 9b). The field intensity at the receiver is the same as at ~22 m in front of the subject (Supplementary Fig. 9c); this eavesdropping range cannot be reduced by power control without compromising communication between the wearable devices. In contrast, metamaterial textiles localized the wireless signal within 10 cm of the body, enabling efficient transmission around the body without radiation into the surrounding space (Supplementary

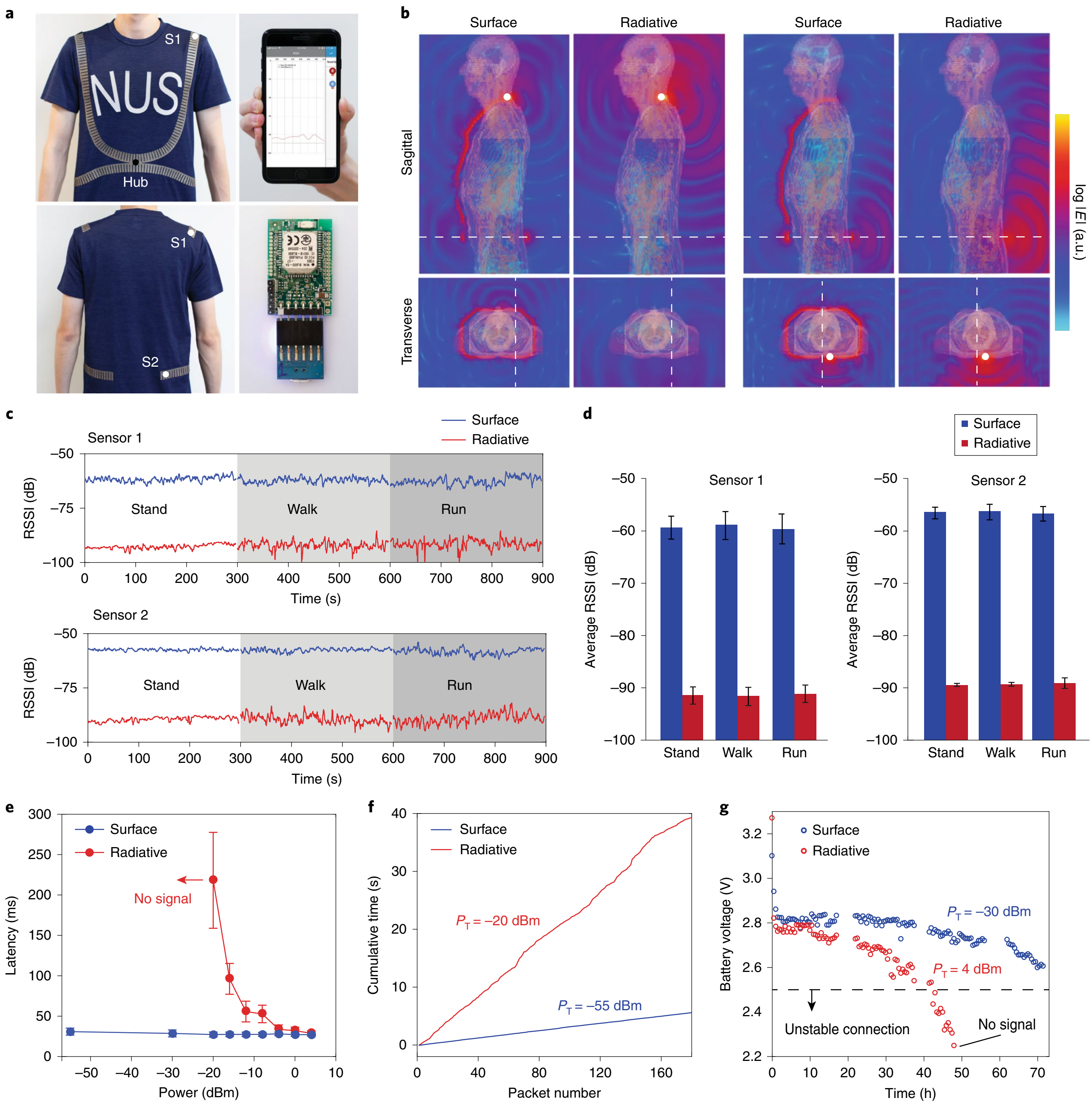

Fig. 3 | Energy-efficient wireless communication on the body. a, Wireless network of two Bluetooth sensor nodes (S1 and S2) simultaneously transmitting data to a smartphone (hub). The devices are worn above the shirt. **b**, Full-wave simulations of wireless transmission in a computational human body model. Dashed lines show the cutting planes and white dots the transmitting sensor. **c**, RSSI was recorded by the smartphone from each sensor during physiological activity. **d**, Comparison of RSSI averaged across each activity. Error bars show s.d. ($n=3$ subjects). **e**, Wireless transmission (Bluetooth) latency as a function of transmit power. Error bars show s.d. ($n=60$ packets). **f**, Cumulative transmission time as a function of number of packets. **g**, Battery lifetime of the sensor nodes during continuous Bluetooth transmission. The received power level is the same for both configurations.

Fig. 9b). This physical-layer security can complement cryptography and protocol-based approaches because it requires no additional computation or modification of the wireless device.

To experimentally demonstrate the localization of signals on the body, we measured the wireless signal strength as a function of distance from the body during Bluetooth interconnection of two sensor nodes worn on the body (Fig. 4a). Figure 4b shows the signal strength from each sensor node measured by an eavesdropper near the subject, both wearing and and not wearing the metamaterial textiles. Without the metamaterial textiles, wireless communication is radiative and is partially obstructed by the body, which results in an increase in signal strength for a distance up to 20 cm from the body. At larger distances, the signal decays due to radiative losses, and the signal strength is comparable whether on the body or 2.5 m away from the subject. Wireless interconnection with the metamaterial textiles, in contrast, exhibits an exponential decay in signal

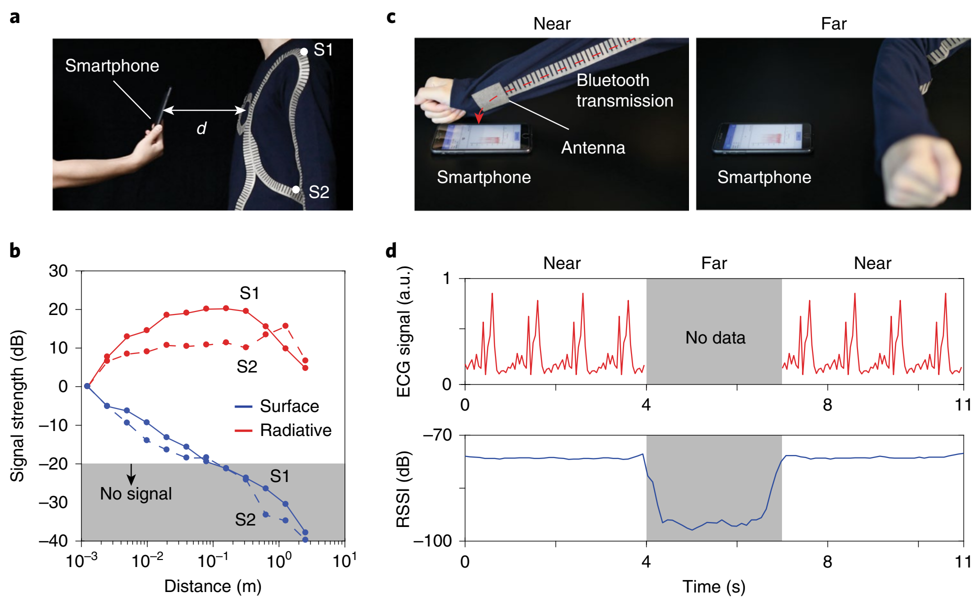

Fig. 4 | Secure wireless body sensor networks. a, Wireless communication between two sensor nodes (labelled S1 and S2) and a smartphone at distance *d* from the body (Supplementary Video 1). **b**, Signal strength recorded at the position of the smartphone as a function of *d*. **c**, Bluetooth transmission of the ECG waveform along the sleeve to a textile-integrated antenna. **d**, ECG signal and Bluetooth RSSI received by the smartphone when the antenna is in the proximity of (near) and moved away (far) from the the smartphone (Supplementary Video 1).

strength with distance. The signal strength falls below thresholds for communication at a distance of 10 cm while maintaining wireless interconnection between the sensor nodes.

As an example of secure Bluetooth data transfer, we demonstrated wireless transmission of electrocardiography (ECG) data along a sleeve integrated with an antenna near the wrist (Fig. 4c). The data can be wirelessly transmitted to the phone only when the wrist is placed a few centimetres above a smartphone; motion of the wrist away from the smartphone results in no detectable signal (Fig. 4d). Furthermore, the localization of wireless signals on the body can suppress interference between neighbouring networks and reduce spectrum-sharing requirements. Supplementary Fig. 10 shows an illustrative example in which communication between two devices on the body is subject to interference by an external device transmitting at the same power level. The signal-to-interference ratio (SIR) exceeds 20 dB when the interfering device is at a distance greater than 20 cm. Such personal networks that are immune to interference could enable individual utilization of full radio bands without degradation of performance from nearby devices.

Wireless power transfer and touch sensing

The efficient propagation of radio surface plasmons on metamaterial textiles enables wireless power transfer to many classes of low-power sensor. As a demonstrative example, we wirelessly powered a pulse indicator on the wrist by guiding energy along a long-sleeved sweater along the length of the arm (Fig. 5a,b). When powered, the pulse indicator provides a visual indication of the subject's heartbeat because the intensity of the light-emitting diode (LED) is modulated by a resistive pressure sensor (Supplementary Fig. 11) that senses pulsation on the wrist of the user (see Methods). The transmitter was placed on the shoulder and the output power set to 20 dBm (100 mW, equivalent to a WiFi transmitter). Monitoring the LED brightness during wireless power transfer shows that the pulses correspond to periodic cardiac activity recorded by ECG (Fig. 5c). The transfer efficiency in this configuration is estimated to be 10.5% to the loop antenna and, including losses due to the rectifier, 3.5% to the LED (Supplementary Fig. 12). These power levels meet requirements for many low-power sensors, including temperature, pH and other physiological markers, which consume less than 1 mW (ref. [26]).

To demonstrate that wireless, battery-free sensors can be interconnected within our platform, we wirelessly powered Bluetooth sensor nodes placed on the shoulder and on the wrist along the metamaterial textile. The sensor circuit is powered by a custom wireless energy harvesting unit (Fig. 5b) and integrates a temperature sensor, a humidity sensor and a Bluetooth module that wirelessly transmits data to a smartphone placed near the body (Fig. 5d). Touching the sensors results in an increase in temperature and humidity, which can be detected by the respective sensors and displayed by an application on the smartphone (Fig. 5e and Supplementary Fig. 13). The distributed and synchronized capabilities of such wireless sensor networks could be used to monitor clinically important physiological signals such as pulse pressure propagation and electrical activity.

The interaction of surface waves with nearby objects also provides sensing capabilities in analogy to optical plasmonic sensors[28]. To demonstrate the potential of our platform for human–machine interaction, we created an interactive smartphone application that changes the display image when an abrupt change in Bluetooth RSSI is detected (Fig. 5f). When the smartphone is placed near a metamaterial textile on which a Bluetooth signal is propagating, the display image can be changed by touching the textile with the index finger, even if the smartphone and the finger are not both in physical contact with the textile (Fig. 5g and Supplementary Video 2). Our measurements show that the proximity of the textiles to biological tissue decreases the transmission by up to 6 dB, due to interaction with the surface wave (Supplementary Fig. 14). By tailoring the geometry of the metamaterial structure to modify the localization of the surface plasmons, this sensitivity to the proximity of biological tissue could be suppressed to improve robustness to environmental effects, or further enhanced for applications in gesture sensing, proximity detection and physiological monitoring.

Conclusions

We have demonstrated the energy-efficient and secure interconnection of wireless sensor networks by confining radio-waves emitted

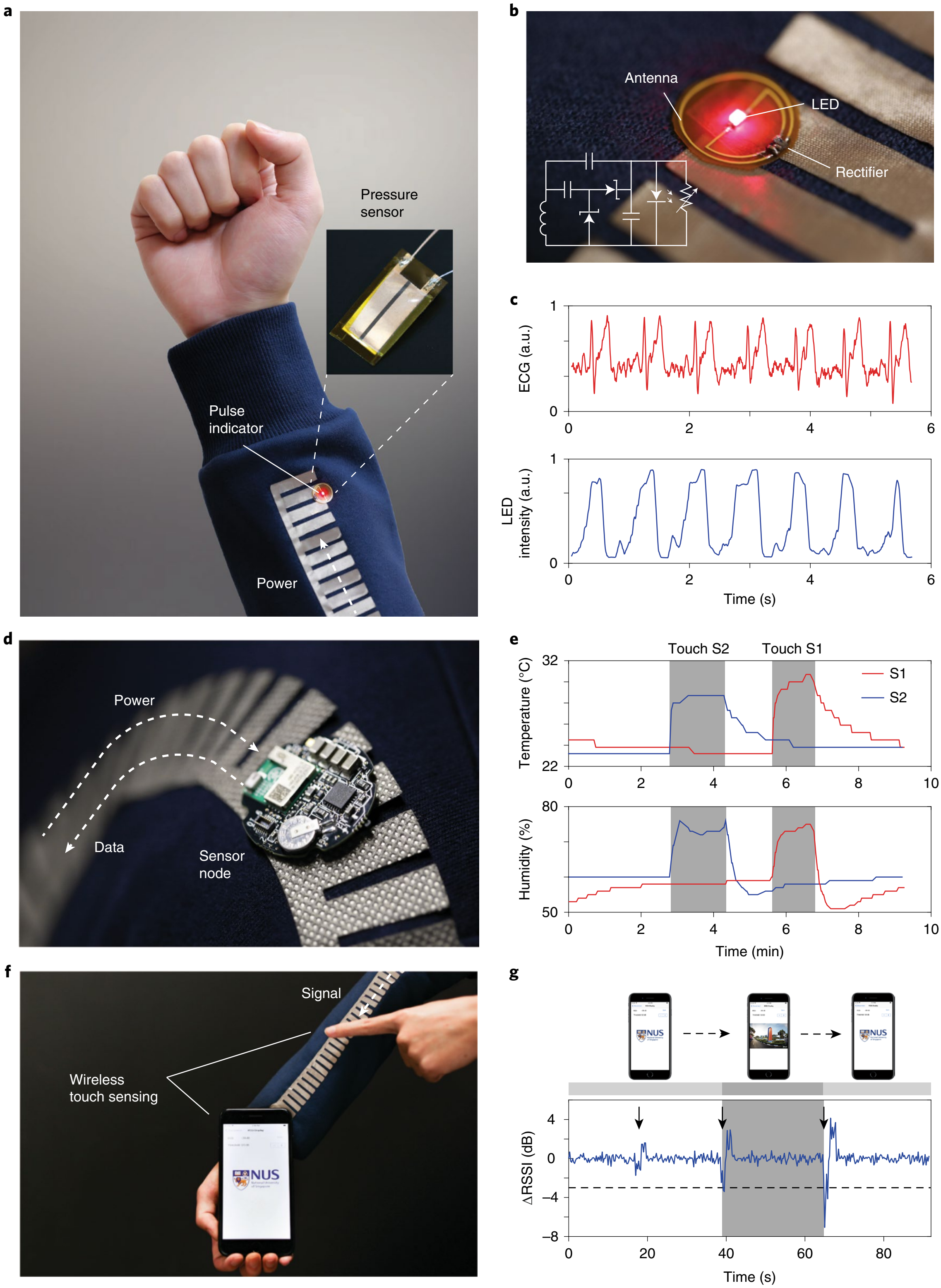

Fig. 5 | Textile-based wireless power transfer and touch sensing. a, Image of a wrist-worn pulse sensor wirelessly powered by signal propagating along the sleeve. The pulse sensor comprises an energy harvesting unit, pressure sensor and LED for visual indication. The pressure sensor is placed under the textile on the wrist. **b**, Image of the energy harvesting unit on the metamaterial textile and its circuit schematic. The pressure sensor is represented by the variable resistor. **c**, Wirelessly powered LED intensity during pulse detection. The recorded ECG is shown for comparison. **d**, Battery-free, wirelessly powered Bluetooth sensor node. **e**, Data recorded on a smartphone from wireless sensor nodes placed on the shoulder (S1) and on the wrist (S2). The shaded regions indicate intervals when the sensor is touched. **f**, Wireless textile-based touch sensing using the Bluetooth protocol (Supplementary Video 2). **g**, Instantaneous change in RSSI and image displayed on the smartphone application when the index finger is placed near the metamaterial textile (black arrows). The dashed line shows the threshold for change in the displayed image.

by standard wireless devices onto metamaterial textiles. We show that the transmission efficiency of a wireless network can be enhanced by over three orders of magnitude compared to conventional radiative networks without metamaterial textile. Furthermore, we have demonstrated the wireless transmission of personal health data along a sleeve near the wrist and shown that Bluetooth signals can be localized to within 10 cm of the body. We have also shown that our metamaterial textiles can support the robust propagation of wireless signals, even across discontinuities in the conductive structure, and enable networks with new capabilities in wireless power transfer and wireless touch sensing. Our results highlight the potential of using clothing to engineer electromagnetic propagation around the body and provide a starting point for the translation of concepts from microwave and photonic circuits onto a textile platform for wireless sensing, signal processing and energy transfer. We envision that endowing athletic wear, medical clothing and other apparel with such advanced electromagnetic capabilities can enhance our ability to perceive and interact with the world around us.

Methods

Metamaterial textile design. The metamaterial shown in Fig. 2a supports a surface plasmon dispersion of the form

$$\beta = \frac{\omega}{c}\sqrt{\frac{\varepsilon_1\varepsilon_2}{\varepsilon_1+\varepsilon_2}}$$

where ε_1 is the permittivity of the dielectric and ε_2 is the permittivity of the metal. Using the Drude model without damping, ε_2 can be modelled as $\varepsilon_2 = 1-\frac{\omega_p^2}{\omega^2}$ where ω_p is a parameter analogous to the plasma frequency. The metamaterial has a negative permittivity parameter $\varepsilon_2 < 0$ at frequencies $\omega < \omega_p$. The resulting dispersion curve lies right of the light line and approaches a horizontal asymptote $\omega = \omega_{sp}$, where $\omega_{sp} = \omega_p/\sqrt{1+\varepsilon_1}$ is the surface plasma frequency. The parameters ε_1 and ω_p for the metamaterial textile can be found by fitting the numerically calculated dispersion curve to this model.

The metamaterial textile is designed by determining the geometrical parameters of the structure to support a surface mode with a desired wavenumber β_s at the design frequency $f_0 = 2.4$ GHz. The resulting surface plasmon wavelength is given by $\lambda_{sp} = 2\pi/\beta_s$ and the decay length $\alpha_1^{-1} = 1/\sqrt{\beta_s^2-(\omega/c)^2}$, which determines the distance at which wireless devices can interact with the textile. The design procedure (Supplementary Fig. 1a) proceeds as follows. (1) The length of the unit cell is set to $d = 0.2\lambda_s$. Simulations show that d has negligible effect on β_s if it is significantly subwavelength (Supplementary Fig. 1d), while larger values result in designs that are easier to fabricate. (2) The parameters of the comb-like structure are set as $a = 0.5d$ and $b = 0.75d$. Supplementary Fig. 1b,c shows that β_s is largely insensitive to a and b but can be tuned over a broad range by h. (3) Parameter h is initialized to $h_0 = \pi c/(4\pi\varepsilon_{tex} f_0)$, where ε_{tex} is the relative dielectric permittivity of the textile. (4) The width of the bottom textile layer is set to $w = a + h$. This design suppresses nearly all coupling to the body (Supplementary Fig. 15) while minimizing the area of conductive textile required (Supplementary Fig. 16). (5) Given the thickness of the textile, t_f, the dispersion curve of the structure is obtained by an eigenmode solver with varying h between $0.5h_0$ and $2h_0$, yielding the value for which $\beta = \beta_s$. The designed metamaterial textile supports the dispersion curve shown in Fig. 1h and fits the surface plasmon model with parameters $\varepsilon_1 = 4$ and $\omega_p = 3.75\times10^{10}$ rad m^{-1}.

Numerical simulations. Electromagnetic simulations were carried out with CST Microwave Studio (Dassault Systems). Field distributions were calculated using the finite-difference time-domain method using dipole excitation. Materials were assigned properties $\varepsilon_{tex} = 1.5$ for textiles and $\varepsilon_{body} = 40$ for tissue, while the computational body model used an anatomically accurate voxel model (Laura, CST Voxel Family) with resolution of 1.875 × 1.875 × 1.25 mm. Dispersion curves were obtained by defining a unit cell of the structure and solving for the eigenfrequencies with periodic boundary conditions in the longitudinal directions and phase shift varying from 0 to π.

Metamaterial textiles. Conductive textile patterns were laser-cut (Universal Laser Systems, VLS 2.30) from adhesive Cu/Ni polyester fabric sheets (Conductive Fabric Tape 86750, Laird Technologies; Conductive Non-woven Fabric 4770, Holland Shielding Systems). Patterns were attached on a cotton–polyester blend athletic shirt for radio-wave device and wireless communication experiments, and a cotton sweater for the wireless powering experiments.

Field measurements. Field mapping experiments used an electric field probe mounted on a three-dimensional positioning system (RSE644, Detectus). Signals from the probe were measured by a spectrum analyser as the probe was scanned 5 mm above the textile surface with 2 mm step size. Continuous-wave excitation was performed using a dipole with 1 cm length placed 2 mm above the input position, driven by a signal generator (Model 835, Berkeley Nucleonics).

Transmission measurements. Transmission was measured as $|S_{21}|$ between two identical 1-inch short antennas (2.4 GHz, RN-SMA-S-RP, Microchip Technologies) connected to a vector network analyser (PicoVNA 106, Pico Technology) using coaxial cables (SMA-SMA, 50 Ω, Amphenol). The spacing between the antennas and the textile surface was set to 2 mm using foam separators.

Wireless communication. Wireless communication was performed using the Bluetooth low energy (BLE) protocol. Sensor nodes made use of single-mode Bluetooth v4.0 modules (BL600, Laird Technologies) configured with an integrated antenna, a coin cell battery adapter (BA600, Laird Technologies) and a 3 V lithium battery (CR1632, Energizer). Sensors transmitted to a central hub consisting of an Android smartphone running a connectivity application (nRF Connect, Nordic Semiconductor) that recorded the signal strength from each sensor. Latency measurements were performed using connectivity testing software (UwTerminalX, Laird Technologies) run from a laptop connected to a hub device (BL620, Laird Technologies) wirelessly connected to the sensor nodes.

Wireless power transfer. Wireless power transfer used a 1-inch short antenna (RN-SMA-S-RP, Microchip Technologies) placed on the textile surface for power transmission. The antenna was driven by a 2.4 GHz signal input directly from a signal generator (SMB100A, Rohde and Schwarz) at 20 dBm (100 mW). The wireless energy harvesting unit was implemented using flexible printed circuit boards (PCBs) integrating the loop antenna and interconnection traces, fabricated commercially (0.1-mm-thick polyimide, 0.5 oz Cu, Gold Phoenix Printed Circuit Board). The rectifier was assembled on a rigid PCB (R4-TG130 substrate, 1 oz Ag, Interhorizon Corporation Pte) by microsoldering (NAE-2A, JBC) the following components: (1) 10 pF capacitor (Johanson Technology, 250R05L100GV4T), (2) 10 nF capacitor (Murata Electronics, GRM0335C1HR20WA01D), (3) 0.2 pF capacitor (Murata Electronics, GRM0335C1ER50BA01D) and (4) Schottky diode (Skyworks, SMS7621-060). The PCBs were integrated together with a red LED chip (Lumex, SML-LX0603SRW-TR) by microsoldering. The pressure sensor was connected in parallel with the LED by copper wire to yield the wireless pulse sensor device.

On-body evaluation. Evaluation of wireless sensor networks on the body was performed with six healthy subjects (three females and three males), aged 20 to 40 years, recruited from the National University of Singapore campus through advertisement by posted notices. Subjects wore an athletic shirt integrated with metamaterial textiles with sensors attached on the back and shoulder, and a smartphone worn over the shirt above the abdomen using a waistband. The smartphone recorded the receive signal strength during indoor physiological activity (standing, walking and running) in 5 min trials with a 2 min rest period in between each trial. Controls were performed by repeating the activity protocol with an unpatterned athletic shirt.

Evaluation of the wirelessly powered sensor was performed with one healthy volunteer. The subject was asked sit back and relax on a chair while a custom pulse sensor was attached to a wrist and electrodes on the arm (Red Dot Electrodes, 3M). The antenna was attached on a long-sleeved sweater integrated with metamaterial textiles at the shoulder and driven with a continuous-wave signal. For quantification, the light intensity from the pulse sensor was measured by using optical fibre connected to a Si amplifier detector (PDA26A-EC, Thorlabs). ECG measurements were simultaneously obtained from the electrodes using a custom amplifier[29]. ECG and optical data were simultaneously recorded using a digital oscilloscope (PicoScope 6402D, Pico Technology).

All experiments complied with a protocol approved by the National University of Singapore Institutional Review Board (N-18-069). All subjects were volunteers, were informed of risks and benefits, and provided informed consent.

Sensor design and fabrication. *Pressure sensor.* Microstructured pyramid films[30] were fabricated from a 20:1 mixture of polydimethylsiloxane (PDMS) elastomer base and curing agent (Sylgard 184, Dow Corning). Polyethylene terephthalate (PET) film with 12 μm thickness was used as the substrate. The PDMS mixture was mixed for 1 min at 2,500 r.p.m. using a SpeedMixer (FlackTek) and transferred onto a silicon wafer mould pretreated with octadecyltrichlorosilane. The mixture was spin-coated on the mould at 1,000 r.p.m. for 30 s. A plasma-treated PET film substrate was placed on top of the degassed PDMS film and thermally cured for 4 h. The moulded PDMS film on the PET substrate was plasma-treated and coated with a thin layer of PEDOT:PSS (CLEVIOS PH1000; Heraues) that was premixed with 5 wt% DMSO and 0.1 wt% Zonyl FS-300. The conductive layer was dried in a 70 °C oven for 30 min before use. The pressure sensor was placed on top of the etched copper electrodes and sealed.

Wirelessly powered, battery-free Bluetooth sensors. The sensor nodes were made from commercial BLE sensors (CYALKIT-E02) with an integrated power management component (S6AE103A) and temperature and humility sensors (Si7020-A20). The output terminals of the rectifier in the wireless energy harvesting unit were connected to the input of the power management component on the back side of the sensor. The sensors were attached onto the metamaterial textile with the antenna of the energy harvesting unit facing down and configured to transmit sensor data via BLE immediately when powered on. The data were wirelessly received using a smartphone and displayed using an application.

Reporting Summary. Further information on research design is available in the Nature Research Reporting Summary linked to this article.

Data availability

The data that support the plots within this paper and other findings of this study are available from the corresponding author upon reasonable request.

Received: 18 September 2018; Accepted: 14 May 2019;
Published online: 17 June 2019

References

1. Kim, D.-H. et al. Epidermal electronics. *Science* **333**, 838–843 (2011).
2. Wang, C. et al. User-interactive electronic skin for instantaneous pressure visualization. *Nat. Mater.* **12**, 899–904 (2013).
3. Tee, B. C. K. et al. Tunable flexible pressure sensors using microstructured elastomer geometries for intuitive electronics. *Adv. Funct. Mater.* **24**, 5427–5434 (2014).
4. Xu, S. et al. Soft microfluidic assemblies of sensors, circuits and radios for the skin. *Science* **344**, 70–74 (2014).
5. Kim, J. et al. Battery-free, stretchable optoelectronic systems for wireless optical characterization of the skin. *Sci. Adv.* **2**, e1600418 (2016).
6. Gao, W. et al. Fully integrated wearable sensor arrays for multiplexed in situ perspiration analysis. *Nature* **529**, 509–514 (2016).
7. Someya, T., Bao, Z. & Malliaras, G. G. The rise of plastic bioelectronics. *Nature* **540**, 379–385 (2016).
8. Han, S. et al. Battery-free, wireless sensors for full-body pressure and temperature mapping. *Sci. Transl. Med.* **10**, eaan4950 (2018).
9. Yang, G.-Z. *Body Sensor Networks* (Springer, 2006).
10. Chu, B., Burnett, W., Chung, J. W. & Bao, Z. Bring on the bodyNET. *Nature* **549**, 328–330 (2017).
11. Takamatsu, S. et al. Wearable keyboard using conducting polymer electrodes on textiles. *Adv. Mater.* **28**, 4485–4488 (2015).
12. Weng, W., Chen, P., He, S., Sun, X. & Peng, H. Smart electronic textiles. *Angew. Chem.* **55**, 6140–6169 (2016).
13. Miyamoto, A. et al. Inflammation-free, gas-permeable, lightweight, stretchable on-skin electronics with nanomeshes. *Nat. Nanotechnol.* **12**, 907–913 (2017).
14. Cao, H., Leung, V., Chow, C. & Chan, H. Enabling technologies for wireless body area networks: a survey and outlook. *IEEE Commun. Mag.* **47**, 84–93 (2009).
15. Li, M., Lou, W. & Ren, K. Data security and privacy in wireless body area networks. *IEEE Wireless Commun.* **17**, 51–58 (2010).
16. Ullah, S. et al. A comprehensive survey of wireless body area networks. *J. Med. Syst.* **36**, 1065–1094 (2010).
17. Pitarke, J. M., Silkin, V. M., Chulkov, E. V. & Echenique, P. M. Theory of surface plasmons and surface-plasmon polaritons. *Rep. Prog. Phys.* **70**, 1–87 (2007).
18. Fang, Y. & Sun, M. Nanoplasmonic waveguides: towards applications in integrated nanophotonic circuits. *Light Sci. Appl.* **4**, e294 (2015).
19. Pendry, J. B., Martn-Moreno, L. & Garcia-Vidal, F. J. Mimicking surface plasmons with structured surfaces. *Science* **305**, 847–848 (2004).
20. Hibbins, A. P., Evans, B. R. & Sambles, J. R. Experimental verification of designer surface plasmons. *Science* **308**, 670–672 (2005).
21. Shen, X., Cui, T. J., Martin-Cano, D. & Garcia-Vidal, F. J. Conformal surface plasmons propagating on ultrathin and flexible films. *Proc. Natl Acad. Sci. USA* **110**, 40–45 (2013).
22. Jackson, J. D. *Classical Electrodynamics* (Wiley, 1999).
23. Zhang, H. C. et al. Broadband amplification of spoof surface plasmon polaritons at microwave frequencies. *Laser Photon. Rev.* **9**, 83–90 (2014).
24. Pozar, D. M. *Microwave Engineering* (Wiley, 2009).
25. Moro, R., Agneessens, S., Rogier, H., Dierck, A. & Bozzi, M. Textile microwave components in substrate integrated waveguide technology. *IEEE Trans. Microw. Theory Tech.* **63**, 422–432 (2015).
26. Chandrakasan, A. P., Verma, N. & Daly, D. C. Ultralow-power electronics for biomedical applications. *Annu. Rev. Biomed. Eng.* **10**, 247–274 (2008).
27. Mercier, P. P. & Chandrakasan, A. P. *Ultra-low-power Short-range Radios* (Springer, 2015).
28. Maier, S. A. & Atwater, H. A. Plasmonics: localization and guiding of electromagnetic energy in metal/dielectric structures. *J. Appl. Phys.* **98**, 011101 (2005).
29. Ng, K. A. et al. An inductively powered CMOS multichannel bionic neural link for peripheral nerve function restoration. *Proc. IEEE Asian Solid State Circuits Conf.* 181–184 (2012).
30. Mannsfeld, S. C. B. et al. Highly sensitive flexible pressure sensors with microstructured rubber dielectric layers. *Nat. Mater.* **9**, 859–864 (2010).

Acknowledgements

The authors thank Z. Goh for assistance with the art in Fig. 1. J.S.H. acknowledges support from National Research Foundation Singapore (NRFF2017-07) and an NUS Young Investigator Award. B.C.K.T. acknowledges support from National Research Foundation Singapore (NRFF2017-08) and an NUS Startup Grant. Both J.S.H. and B.C.K.T. acknowledge support from Institute for Health Innovation and Technology grants. X.T., H.Y. and Z.L. acknowledge support from the NUS Research Scholarship.

Author contributions

X.T., P.M.L., B.C.K.T. and J.S.H. conceived and planned the research. X.T., P.M.L., Y.J.T., T.L.Y.W., H.Y., M.Z., Z.L., K.A.N. and J.S.H. designed the metamaterial textiles, sensor nodes and performed the experiments. X.T., P.M.L. and J.S.H. wrote the paper with input from all the authors.

Competing interests

The authors declare no competing interests.

Additional information

Supplementary information is available for this paper at https://doi.org/10.1038/s41928-019-0257-7.

Reprints and permissions information is available at www.nature.com/reprints.

Correspondence and requests for materials should be addressed to J.S.H.

nature research

Corresponding author(s): John S. Ho

Last updated by author(s): May 14, 2019

Reporting Summary

Nature Research wishes to improve the reproducibility of the work that we publish. This form provides structure for consistency and transparency in reporting. For further information on Nature Research policies, see Authors & Referees and the Editorial Policy Checklist.

Statistics

For all statistical analyses, confirm that the following items are present in the figure legend, table legend, main text, or Methods section.

n/a	Confirmed	
☐	☒	The exact sample size (*n*) for each experimental group/condition, given as a discrete number and unit of measurement
☐	☒	A statement on whether measurements were taken from distinct samples or whether the same sample was measured repeatedly
☒	☐	The statistical test(s) used AND whether they are one- or two-sided *Only common tests should be described solely by name; describe more complex techniques in the Methods section.*
☒	☐	A description of all covariates tested
☒	☐	A description of any assumptions or corrections, such as tests of normality and adjustment for multiple comparisons
☐	☒	A full description of the statistical parameters including central tendency (e.g. means) or other basic estimates (e.g. regression coefficient) AND variation (e.g. standard deviation) or associated estimates of uncertainty (e.g. confidence intervals)
☒	☐	For null hypothesis testing, the test statistic (e.g. *F*, *t*, *r*) with confidence intervals, effect sizes, degrees of freedom and *P* value noted *Give P values as exact values whenever suitable.*
☒	☐	For Bayesian analysis, information on the choice of priors and Markov chain Monte Carlo settings
☒	☐	For hierarchical and complex designs, identification of the appropriate level for tests and full reporting of outcomes
☒	☐	Estimates of effect sizes (e.g. Cohen's *d*, Pearson's *r*), indicating how they were calculated

Our web collection on statistics for biologists contains articles on many of the points above.

Software and code

Policy information about availability of computer code

Data collection	Bluetooth data was collected using commercial connectivity analysis software (UwTerminalX, Laird Technologies and nRF Connect, Nordic Semiconductor). Electromagnetic simulations used the finite-difference time-domain method using commercial software (CST Microwave Studio, Dassault Systems).
Data analysis	The plots in this manuscript were generated using MATLAB (version R2017a). No custom data analysis was performed.

For manuscripts utilizing custom algorithms or software that are central to the research but not yet described in published literature, software must be made available to editors/reviewers. We strongly encourage code deposition in a community repository (e.g. GitHub). See the Nature Research guidelines for submitting code & software for further information.

Data

Policy information about availability of data

All manuscripts must include a data availability statement. This statement should provide the following information, where applicable:

- Accession codes, unique identifiers, or web links for publicly available datasets
- A list of figures that have associated raw data
- A description of any restrictions on data availability

The data that support the plots within this paper and other findings of this study are available from the corresponding author upon reasonable request.

Field-specific reporting

Please select the one below that is the best fit for your research. If you are not sure, read the appropriate sections before making your selection.

☐ Life sciences ☐ Behavioural & social sciences ☐ Ecological, evolutionary & environmental sciences

For a reference copy of the document with all sections, see nature.com/documents/nr-reporting-summary-flat.pdf

Life sciences study design

All studies must disclose on these points even when the disclosure is negative.

Sample size	*Describe how sample size was determined, detailing any statistical methods used to predetermine sample size OR if no sample-size calculation was performed, describe how sample sizes were chosen and provide a rationale for why these sample sizes are sufficient.*
Data exclusions	*Describe any data exclusions. If no data were excluded from the analyses, state so OR if data were excluded, describe the exclusions and the rationale behind them, indicating whether exclusion criteria were pre-established.*
Replication	*Describe the measures taken to verify the reproducibility of the experimental findings. If all attempts at replication were successful, confirm this OR if there are any findings that were not replicated or cannot be reproduced, note this and describe why.*
Randomization	*Describe how samples/organisms/participants were allocated into experimental groups. If allocation was not random, describe how covariates were controlled OR if this is not relevant to your study, explain why.*
Blinding	*Describe whether the investigators were blinded to group allocation during data collection and/or analysis. If blinding was not possible, describe why OR explain why blinding was not relevant to your study.*

Behavioural & social sciences study design

All studies must disclose on these points even when the disclosure is negative.

Study description	*Briefly describe the study type including whether data are quantitative, qualitative, or mixed-methods (e.g. qualitative cross-sectional, quantitative experimental, mixed-methods case study).*
Research sample	*State the research sample (e.g. Harvard university undergraduates, villagers in rural India) and provide relevant demographic information (e.g. age, sex) and indicate whether the sample is representative. Provide a rationale for the study sample chosen. For studies involving existing datasets, please describe the dataset and source.*
Sampling strategy	*Describe the sampling procedure (e.g. random, snowball, stratified, convenience). Describe the statistical methods that were used to predetermine sample size OR if no sample-size calculation was performed, describe how sample sizes were chosen and provide a rationale for why these sample sizes are sufficient. For qualitative data, please indicate whether data saturation was considered, and what criteria were used to decide that no further sampling was needed.*
Data collection	*Provide details about the data collection procedure, including the instruments or devices used to record the data (e.g. pen and paper, computer, eye tracker, video or audio equipment) whether anyone was present besides the participant(s) and the researcher, and whether the researcher was blind to experimental condition and/or the study hypothesis during data collection.*
Timing	*Indicate the start and stop dates of data collection. If there is a gap between collection periods, state the dates for each sample cohort.*
Data exclusions	*If no data were excluded from the analyses, state so OR if data were excluded, provide the exact number of exclusions and the rationale behind them, indicating whether exclusion criteria were pre-established.*
Non-participation	*State how many participants dropped out/declined participation and the reason(s) given OR provide response rate OR state that no participants dropped out/declined participation.*
Randomization	*If participants were not allocated into experimental groups, state so OR describe how participants were allocated to groups, and if allocation was not random, describe how covariates were controlled.*

Ecological, evolutionary & environmental sciences study design

All studies must disclose on these points even when the disclosure is negative.

Study description	*Briefly describe the study. For quantitative data include treatment factors and interactions, design structure (e.g. factorial, nested, hierarchical), nature and number of experimental units and replicates.*
Research sample	*Describe the research sample (e.g. a group of tagged Passer domesticus, all Stenocereus thurberi within Organ Pipe Cactus National*

Research sample	*Monument), and provide a rationale for the sample choice. When relevant, describe the organism taxa, source, sex, age range and any manipulations. State what population the sample is meant to represent when applicable. For studies involving existing datasets, describe the data and its source.*
Sampling strategy	*Note the sampling procedure. Describe the statistical methods that were used to predetermine sample size OR if no sample-size calculation was performed, describe how sample sizes were chosen and provide a rationale for why these sample sizes are sufficient.*
Data collection	*Describe the data collection procedure, including who recorded the data and how.*
Timing and spatial scale	*Indicate the start and stop dates of data collection, noting the frequency and periodicity of sampling and providing a rationale for these choices. If there is a gap between collection periods, state the dates for each sample cohort. Specify the spatial scale from which the data are taken*
Data exclusions	*If no data were excluded from the analyses, state so OR if data were excluded, describe the exclusions and the rationale behind them, indicating whether exclusion criteria were pre-established.*
Reproducibility	*Describe the measures taken to verify the reproducibility of experimental findings. For each experiment, note whether any attempts to repeat the experiment failed OR state that all attempts to repeat the experiment were successful.*
Randomization	*Describe how samples/organisms/participants were allocated into groups. If allocation was not random, describe how covariates were controlled. If this is not relevant to your study, explain why.*
Blinding	*Describe the extent of blinding used during data acquisition and analysis. If blinding was not possible, describe why OR explain why blinding was not relevant to your study.*

Did the study involve field work? ☐ Yes ☐ No

Field work, collection and transport

Field conditions	*Describe the study conditions for field work, providing relevant parameters (e.g. temperature, rainfall).*
Location	*State the location of the sampling or experiment, providing relevant parameters (e.g. latitude and longitude, elevation, water depth).*
Access and import/export	*Describe the efforts you have made to access habitats and to collect and import/export your samples in a responsible manner and in compliance with local, national and international laws, noting any permits that were obtained (give the name of the issuing authority, the date of issue, and any identifying information).*
Disturbance	*Describe any disturbance caused by the study and how it was minimized.*

Reporting for specific materials, systems and methods

We require information from authors about some types of materials, experimental systems and methods used in many studies. Here, indicate whether each material, system or method listed is relevant to your study. If you are not sure if a list item applies to your research, read the appropriate section before selecting a response.

Materials & experimental systems

n/a	Involved in the study	
☒	☐	Antibodies
☒	☐	Eukaryotic cell lines
☒	☐	Palaeontology
☒	☐	Animals and other organisms
☐	☒	Human research participants
☒	☐	Clinical data

Methods

n/a	Involved in the study	
☒	☐	ChIP-seq
☒	☐	Flow cytometry
☒	☐	MRI-based neuroimaging

Human research participants

Policy information about studies involving human research participants

Population characteristics	Evaluation of wireless sensor networks on the body was performed with 3 healthy subjects (1 female and 2 males), aged 20 to 40.
Recruitment	Subjects were recruited from the National University of Singapore campus through advertisement by posted notices
Ethics oversight	All experiments complied with protocol approved by the National University of Singapore Institutional Review Board (N-18-069).

Note that full information on the approval of the study protocol must also be provided in the manuscript.